Applied Catalysis B: Environmental 310 (2022) 121354

Contents lists available at ScienceDirect

Applied Catalysis B: Environmental

journal homepage: www.elsevier.com/locate/apcatb

Round-the-clock bifunctional honeycomb-like nitrogen-doped carbon-decorated Co_2P/Mo_2C-heterojunction electrocatalyst for direct water splitting with 18.1% STH efficiency

Pengliang Sun [a,1], Yingtang Zhou [b,1], Hongyi Li [c,1], Hua Zhang [a], Ligang Feng [d,*], Qiue Cao [a], Shixi Liu [a,*], Thomas Wågberg [e], Guangzhi Hu [a,e,**]

[a] School of Chemical Science and Technology, Institute for Ecological Research and Pollution Control of Plateau Lakes, and School of Ecology and Environmental Science, Yunnan University, Kunming 650504, PR China
[b] National Engineering Research Center for Marine Aquaculture, Marine Science and Technology College, Zhejiang Ocean University, Zhoushan 316004, PR China
[c] Guangzhou Panyu Polytechnic, Guangzhou 511483, PR China
[d] School of Chemistry and Chemical Engineering, Yangzhou University, Yangzhou 225009, PR China
[e] Department of Physics, Umeå University, S-901 87 Umeå, Sweden

ARTICLE INFO

Keywords:
Overall water splitting
Heteroatom cooperative coupling
Heterojunction interface
Round-the-clock
Intrinsic activity
Solar-to-hydrogen efficiency

ABSTRACT

Hydrogen production via solar and electrochemical water splitting is a promising approach for storing solar energy and achieving a carbon-neutral economy. However, hydrogen production by photoelectric coupling remains a challenge. Here, by the cooperative coupling of heteroatoms and a heterojunction interface engineering strategy in a limited space, a honeycomb porous Co_2P/Mo_2C@NC catalyst was obtained for the first time. In contrast most traditional chemical syntheses, this method maintains excellent electrical interconnections among the nanoparticles and results in large surface areas and many catalytically active sites. Theoretical calculations reveal that the construction of a heterostructure can effectively lower the hydrogen evolution reaction and oxygen evolution reaction barriers as well as improve the electrical conductivity, consequently enhancing the electrochemical performance. Significantly, the overall water-splitting hydrolytic tank assembled using AsGa solar cells enabled the system to achieve a stable solar hydrogen conversion efficiency of 18.1%, which provides a new approach for facilitating large-scale hydrogen production via portable water hydrolysis driven by solar cells.

1. Introduction

The rapid depletion of fossil fuels and the environmental crisis have strongly stimulated the development of renewable alternative energy sources [1–4]. As a fuel with a zero carbon footprint, hydrogen is considered as a promising substitute for fossil fuels because of its high energy density and cleanliness [5,6]. Photocatalytic and electrocatalytic water splitting have emerged as mainstream research areas in the field of hydrogen production. However, photocatalysis cannot be performed continuously owing to weather reasons (rainy days and dark nights), and electrocatalysis consumes a large amount of electrical energy, which limits its long-term development. However, the combination of photovoltaic and electrochemical hydrogen production can solve the issue of "light abandonment and power consumption" to a large extent. However, water splitting is a thermodynamic uphill process, and the overpotential (η) of the hydrogen evolution reaction (HER) and oxygen evolution reaction (OER) is very high; therefore, efficient and stable electrocatalysts are required to reduce the overpotential significantly [4,7]. In addition, the overall water splitting decomposition driven by solar energy is performed under harsh conditions, such as intermittent and position-dependent solar irradiation, and the conversion rate of solar energy to hydrogen obtained at laboratory scale is still very low [8–10]. Currently, Pt- and Ir/Ru-based compounds are the most advanced HER and OER electrocatalysts, respectively. However, the high price,

* Corresponding authors.
** Corresponding author at: School of Chemical Science and Technology, Institute for Ecological Research and Pollution Control of Plateau Lakes, and School of Ecology and Environmental Science, Yunnan University, Kunming 650504, PR China.
E-mail addresses: ligang.feng@yzu.edu.cn (L. Feng), shxliu@ynu.edu.cn (S. Liu), guangzhihu@ynu.edu.cn (G. Hu).
[1] These authors contributed equally.

https://doi.org/10.1016/j.apcatb.2022.121354
Received 6 February 2022; Received in revised form 10 March 2022; Accepted 24 March 2022
Available online 31 March 2022

scarcity, low bifunctionality, and poor stability of these precious metals significantly limit their wide application [11–13]. Therefore, it is necessary to develop inexpensive, round-the-clock durable, bifunctional, and efficient electrocatalysts as electrode materials for water splitting.

In recent years, *d*-zone transition metal-based catalysts (such as Mo, W, Fe, Co and Ni) have been widely used as HER or OER electrocatalysts for electrochemical water splitting [14–16]. Some transition metal phosphating compounds (TMP), such as CoP [17], Co_2P [8,18], MoP [19], Ni_2P [20,21], FeP [22] etc., are not only efficient HER electrocatalysts but also excellent OER catalysts to achieve integral water splitting. Das et al. [23] proposed a one-step synthesis of Co_2P nanoparticles coated with N-doped carbon nanotubes, and found that the more electronegative P atoms in the Co_2P lattice can capture electrons from the metal atoms and play a crucial role in the HER process. Zhang et al. [24] successfully prepared ultrathin Ga-doped CoP nanowires using electrodeposition and phosphating, which showed excellent HER electrocatalytic activity. This may be due to the unique characteristics of Ga, which can systematically improve the HER activity of CoP by improving the adsorption of H_2O, weakening the adsorption of OH, and optimizing the adsorption/desorption of H. The phosphorus atoms doped into the cobalt lattice play an important role in the HER because phosphorus atoms with a high electronegativity can seize electrons from metal atoms and act as Lewis bases in the HER process, working with positively charged protons [25].

In addition, molybdenum carbide is an important member of the early transition metal carbides. Because its electronic structure is similar to that of platinum group metals, molybdenum carbide has attracted considerable interest as a high-performance HER electrocatalyst [26,27]. However, the unoccupied d orbital of Mo in Mo_2C leads to the formation of a strong Mo–H bond because the H atom contributes its electrons to the neighboring Mo atom, and the strong coupling hinders the HER process [28]. To overcome this issue, a strategy to control the bond energy of Mo–H has been developed to enhance HER dynamics. The catalytic activity of Mo_2C can be improved by heteroatom modification [29], defect manipulation [30], heterostructure modification [26], recombination [31] and morphology control [32]. Among these options, heterostructure strategies, such as the establishment of heterostructures composed of transition metal phosphide and Mo_2C, can promote the rapid desorption of H_2 and accelerate the HER because electrons in transition metals can be transferred to Mo to occupy their d orbitals, thereby increasing the d orbitals occupancy of Mo in Mo_2C. In addition, the heterogeneous interface can promote the splitting of water and further improve the overall water-splitting performance by accelerating OER kinetics. Luo et al. [33] obtained a CoP/Mo_2C-NC hybrid electrocatalyst by coating Co-ZIF-67 on the surface of MoO_3 nanorods and via pyrolysis and phosphating, and its electrocatalytic activity for HER was significantly improved. This is because of the strong chemical coupling between CoP and Mo_2C in CoP/Mo_2C-NC, which leads to the migration of Co electron cloud to Mo, optimizing the hydrogen bonding and HER kinetics. However, the above-mentioned issues result in limitations, such as poor performance and the instability of electrocatalytic water splitting along with a poor performance in the actual application of solar-driven water splitting, which urgently need to be addressed. Therefore, it is of substantial significance to synthesize a novel hybrid catalyst rich in rare-earth transition metal-based carbides and phosphating compounds and improve their electrocatalytic activity. However, the realization of this effective combination remains a significant challenge because phosphating and carbonization cannot easily occur simultaneously in a limited space.

This is inspired by the fact that the heterojunction coupling of Mo_2C can simultaneously improve the intrinsic activity of the HER and accelerate the catalytic kinetics of the OER. In this study, we successfully introduced a direct interfacial interaction between the transition metal phosphide and Mo_2C by the one-step pyrolysis of dopamine (DA)-supported polyoxometalates to obtain a suitable Mo–H bond energy, thereby achieving excellent adsorption and desorption properties for water splitting. To overcome the related difficulties and inspired by its excellent catalytic activity, this study introduces the one-step synthesis of an N-doped carbon-coated Co_2P/Mo_2C heterojunction, and then uses it as an electrocatalyst for both HER and OER, thereby realizing overall water splitting in an alkaline medium. The study of the electrocatalytic mechanism showed that heteroatom doping improved the activity of the catalyst, and the three-dimensional (3D) porous morphology increased the contact area between the catalyst and the electrolyte. An increase in the number of active centers was observed, and the heterostructure realized interfacial charge regulation driven by the Mott–Schottky effect. The all-alkaline electrolytic cell using Co_2P/Mo_2C@NC as anode and cathode catalysts has a cell voltages of approximately 1.55 V at a current density of 10 mA cm^{-2} over a long operating period, which is comparable to the most advanced combination of Pt/C and RuO_2 at present. Furthermore, a stable Solar-to-hydrogen (STH) conversion efficiency of 18.1% was achieved using a solar-driven water-splitting electrolyzer. In this study, a comprehensive cooperative strategy of morphology and heterogeneous interface charge regulation is proposed, which provides a valuable pathway for the design of other water-splitting electrocatalysts.

2. Experimental section

2.1. Chemicals

The detailed preparation process of the SiO_2 nanospheres and $CoPMo_{12}$ is provided in the Supporting material. Other reagents (analytical grade) were purchased from Aladdin Chemical Reagent Co., Ltd. and used as received. Milli-Q ultrapure water (18 MΩ cm^{-1}) was used throughout the experiments.

2.2. Material preparation

2.2.1. Synthesis of Co_2P/Mo_2C@NC

To obtain the crystal SiO_2 @CoPMo@DA complex, 0.2 g $CoPMo_{12}$ and 0.4 g DA were dispersed in 5 mL methanol. Thereafter, 1.0 g SiO_2 nanospheres were ground evenly in a mortar and dried in an oven at 55 °C. After the products were collected, they were ground evenly and heated at 800 °C for 6 h in a N_2 atmosphere to obtain the SiO_2 @CoP-Mo@NC complex. After natural cooling to room temperature, the samples were soaked in 1 M hydrochloric acid for 12 h to remove unstable species and activate them. Subsequently, the product was added to 8.8 mL hydrofluoric acid (10 wt%) solution and stirred at room temperature for 12 h to remove the SiO_2 template. Finally, the powder was washed thoroughly with deionized water and ethanol and dried under vacuum at 50 °C for 12 h. Accordingly, a Co_2P/Mo_2C@NC catalyst was obtained.

2.3. Electrochemical measurements

All electrochemical measurements were performed on a CHI 660E electrochemical workstation coupled with a typical three-electrode system in a 1.0 M KOH solution at room temperature. A catalyst-loaded carbon paper (0.5 cm × 1.0 cm, CP) were used as a working electrode, but the actual immersing area was 0.5 cm × 0.5 cm, while a Hg/HgO electrode and a graphite rod for the HER or Pt wire for the OER were employed as the reference and counter electrodes, respectively. The mass loadings of the catalyst onto CP substrate was approximately 0.25 mg cm^{-2}. The OER and HER performances were recorded using linear sweep voltammetry (LSV) curves in the N_2-saturated electrolyte at a scan rate of 5 mV s^{-1}. For the control experiments, homodisperse commercial RuO_2 and Pt/C (10 mg of powder in 250 μL of ethanol, 700 μL distilled water, and 50 μL of Nafion) were loaded onto the clean CP as working electrodes, with loading amounts equivalent to those of the aforementioned samples. All potentials were converted to the corresponding potentials vs. reversible hydrogen electrode (RHE) using the

equation Evs. RHE = Evs. SCE + 0.0591 × pH + 0.241. All the polarization curves used in this study were corrected for 85% iR compensation. Tafel plots were acquired in linear regions by fitting the Tafel equation ($\eta = a + b \log j$), where η is the overpotential, b is the Tafel slope, and j is the current density. The electrochemical impedance spectroscopy (EIS) studies were conducted in the range of 0.01–105 Hz at an overpotential of 10 mV, with an amplitude perturbation of 5 mV. Double-layer capacitance (C_{dl}) data were obtained using cyclic voltammetry (CV) performed between − 0.7 to − 0.9 V at an increasing sweep rate from 20 to 120 mV s^{-1}. Electrochemical stability tests were performed using multistep chronopotentiometry at current densities of 10, 50, and 100 mA cm^{-2} for 30 h.

2.4. Theoretical calculation

Full computational methods are provided in the Supplemental information.

3. Results and discussion

3.1. Material preparation and characterizations

As a nontoxic and sustainable biomolecule, DA contains both catechol and amino functional groups. DA can polymerize spontaneously under weak alkaline conditions and chelate and adsorb various metal ions during self-polymerization [34,35]. It shows a strong complexing ability for transition metal ions and metal oxygen-containing anions (WO_{42}^-, MoO_{42}^-, etc.) [36–38]. As shown in Fig. 1a, Co_2P/Mo_2C@NC hybrid materials were prepared through the following steps: (1) DA and CoPMo were prepolymerized by a simple solvothermal reaction and then anchored on the surface of SiO_2 beads; (2) DA was fully polymerized and adsorbed CoPMo, and it them calcined to form Co_2P/Mo_2C@NC nanostructures. In the prepolymer solution, DA molecules are adsorbed on the surface of SiO_2 by π–π stacking, while the polyacid clusters on CoPMo are attracted to each other by static electricity and then polymerized in situ.

First, the morphology and structure of the prepared Co_2P/Mo_2C@NC were studied using SEM. The SEM image (Fig. 1b) shows that the porous structure was closely connected and hierarchically distributed. The strong adhesion between the current collector and catalysts is beneficial for reducing the contact resistance, facilitating charge injection and transport from the electrode to the catalyst active site [39]. To further understand the crystallinity and structure of the synthesized Co_2P/Mo_2C@NC catalyst, it was characterized using TEM (Fig. 1c). Significantly, numerous small nanocrystals were dispersed on the porous skeleton. This is conducive to the generation of boundaries, defects, and dislocations, which provide a large number of active centers for improving catalytic activity [16]. As shown in Fig. 1c, the two adjacent

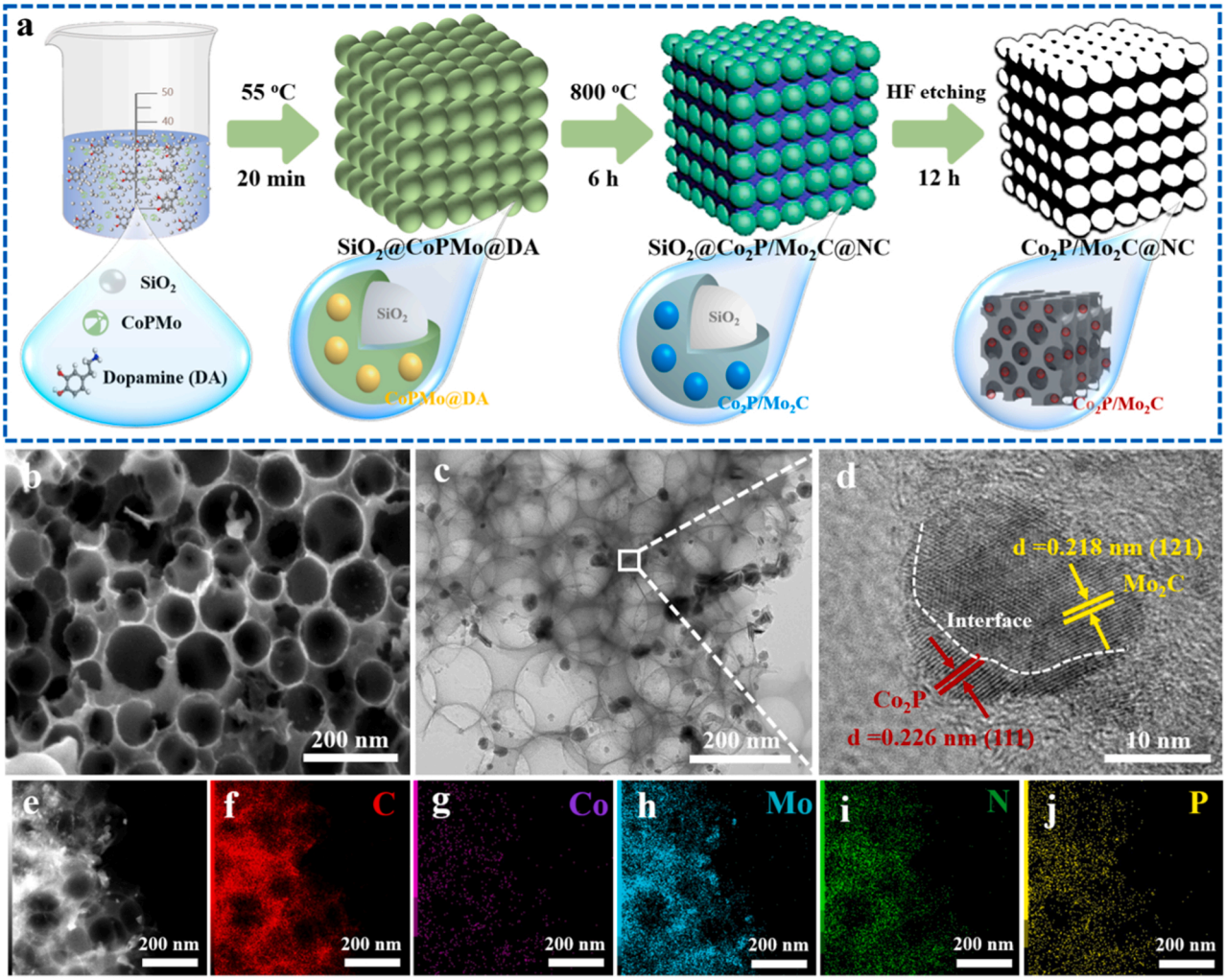

Fig. 1. (a) Schematic of the preparation route of Co_2P/Mo_2C@NC; (b) Scanning electron microscopy (SEM) image of Co_2P/Mo_2C@NC; (c) Transmission electron microscopy (TEM) image of Co_2P/Mo_2C@NC; (d) High-resolution (HR)-TEM image of Co_2P/Mo_2C@NC; (e-j) Distribution mapping of C, Co, Mo, N, and P in Co_2P/Mo_2C@NC.

nanocrystals were closely integrated at the boundary. This indicates that they were closely connected to each other, ensuring a good electrical and mechanical contact, thereby facilitating efficient and stable catalytic reactions. The HR-TEM image (Fig. 1d) shows the detailed structure of the heterostructure and interface. The nanoparticles have lattice stripes with spacings of 0.218 and 0.226 nm, which are attributed to the (121) and (111) planes of Mo_2C and Co_2P, respectively. Clearly, the nanoparticles are highly crystalline heterostructures composed of Mo_2C and Co_2P. Significantly, there was a prominent amorphous interface between the two particles (indicated by the white dotted lines). This shows that the crystal structures of Mo_2C and Co_2P are highly disordered and amorphous. The formation of an amorphous region may alleviate the strain caused by the two highly mismatched lattices of the two phases. It can be assumed that the amorphous interface in the bimetallic heterostructure plays an important role in improving the electrocatalytic activity. In addition, Energy Dispersive X-ray (EDX) spectral element mapping proves the uniform dispersion of Co, Mo, P, N, and C atoms on the entire porous framework (Fig. 1 e–j). Fig. 2a shows the powder X-ray diffraction (PXRD) pattern of Co_2P/Mo_2C@NC. The PXRD peaks can be attributed to a mixture of Co_2P (JCPDS, No. 54–0413) and Mo_2C (JCPDS, No. 31–0871). The peaks at 31.09°, 40.83°, 44.85°, 48.37°, 55.47°, and 67.91° indicate the (110), (111), (021), (120), (030), and (130) crystal planes of Co_2P, respectively. There were four characteristic peaks at 34.41°, 37.94°, 39.45°and 61.38°, which corresponded to the (002), (200), (102), and (040) crystal planes of Mo_2C, respectively. The additional peak observed at 24° can be attributed to graphite carbon [14]. In addition, the Raman spectra further confirm the degree of graphitization of Co_2P/Mo_2C@NC (Fig. 2d). The ratio between the defect (D; 1350 cm^{-1}) and graphitic (G; 1580 cm^{-1}) band intensities (I_D/I_G) was 1.89, implying the presence of partial graphitization and many structural defects on the carbon shells, thereby favoring electroconductivity and H^+/H_2 absorption. Furthermore, to analyze the pore structure of Co_2P/Mo_2C@NC, N_2 adsorption–desorption tests were conducted. From the results shown in Fig. 2(b), the specific surface area of Co_2P/Mo_2C@NC is as high as 88.45 $m^2\ g^{-1}$; its isothermal adsorption is I/IV mixed type, and H4 type hysteresis loop appears in the middle and high pressure regions, indicating that its pore structure is mainly composed of micropores and mesopores. This conclusion can be further confirmed by the pore size distribution results presented in Fig. 2 (c) and Table S1. The interconnected microporous and mesoporous structures can facilitate electrolyte diffusion, and the macro-porous structure can act as an electrolyte reservoir, effectively funneling the reactants and electrolytes into the active sites and enabling the release of bubbles. The XPS survey spectrum confirms the presence of Mo, Co, P, C, N, and O. The high resolution C1s spectrum (Fig. 2e) has a strong peak of C═C (284.5 eV) and three relatively weak peaks of C–N (285.6 eV), C–O (289.2 eV), and C═O (292.2 eV), which indicates the doping of N and O. High-resolution N1S spectra (Fig. 2f) showed that presence of

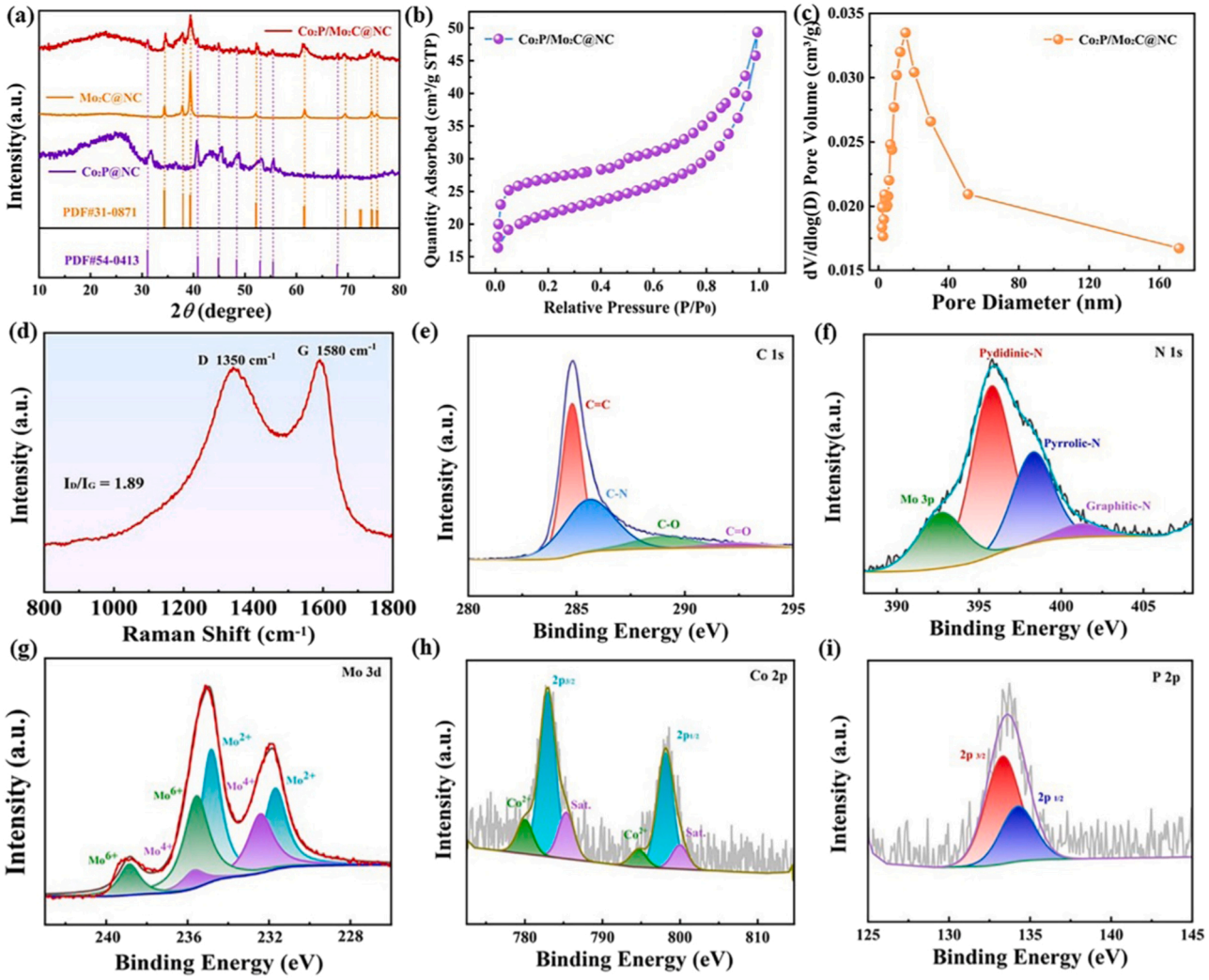

Fig. 2. (a) PXRD pattern; (b) N_2 adsorption-desorption isotherms and (c) pore size distribution of Co_2P/Mo_2C@NC samples; (d) Raman spectra of Co_2P/Mo_2C@NC; HR XPS spectra of (e) C1s, (f) N1s, (g) Mo3d, (h) Co2p, and (i) P2p for Co_2P/Mo_2C@NC.

pyridinic-N (395.8 eV), pyrrolic-N (398.3 eV), and graphitic-N (401.4 eV). The peak at 392.7 eV can be attributed to N associated with the metal (N–Mo bond) and Mo3p. The high resolution P2p spectrum (Fig. 2i) has two peaks at 133.3 eV and 134.2 eV, corresponding to $P2p_{3/2}$ and $P2p_{1/2}$, respectively. The peaks at 782.8 eV and 798.2 eV can be attributed to $Co2p_{3/2}$ and $Co2p_{1/2}$ in Co_2P/Mo_2C@NC (Fig. 2h). The XPS spectrum of Mo3d (Fig. 2g) shows that the Mo element in Co_2P/Mo_2C@NC has + 2, + 4, and + 6 oxidation states [15]. Corresponding to Mo^{2+} (236.30 eV and 233.1 eV), and Mo^{2+} is from molybdenum carbides, which are known to serve as active sites for HER. The high oxidation states of Mo^{4+} (232.4 eV and 235.6 eV) and Mo^{6+} (232.4 eV and 229.2 eV) may be caused by the air-induced surface oxidation of Co_2P/Mo_2C@NC. These oxides can significantly improve the preparation process of HER because the external oxygen atoms can be chemically adsorbed on Mo_2C by replacing carbon atoms, and the chemisorbed oxygen atoms can be used as the active centers of the HER. These results can be used to analyze the charge transfer at the heterogeneous interface of Co_2P/Mo_2C by using the projected density of states (PDOS) and charge density difference in the theoretical calculation part, which shows that the construction of Co_2P/Mo_2C heterogeneous interface significantly enhances the performance of water decomposition.

3.2. Electrocatalytic performances of Co_2P/Mo_2C@NC toward HER

The HER catalytic performance of Co_2P/Mo_2C@NC was investigated in a 1 M KOH electrolyte. For comparison, the HER activities of the benchmark Pt/C, Co_2P @ NC, Mo_2C@NC, and blank CP were also evaluated, as shown in Fig. 3a and c. As expected, the Co_2P/Mo_2C@NC electrode exhibited the highest HER electrochemical activity. The overpotentials required to drive 10 mA cm^{-2}, 50 mA cm^{-2}, and 100 mA cm^{-2} were 86 mV (η10), 133 mV (η50), and 165 mV (η100), respectively, which were comparable to those of the Pt/C electrode (η10 = 37 mV, η50 = 129 mV, and η100 = 218 mV, respectively). Notably, the Co_2P/Mo_2C@NC electrode requires an extremely low overpotential at a high current density of 400 mA cm^{-2}, which is significantly better than that of Pt/C (Fig. 3a illustration). Co_2P/Mo_2C@NC showed better HER activity than Co_2P @ NC and Mo_2C@NC, indicating a synergistic effect between Co_2P and Mo_2C.

In addition, the Co_2P/Mo_2C@NC catalyst exhibited fast kinetic performance for the HER, with a Tafel slope of 46 mV dec^{-1} (Fig. 3b), which was lower than those of Pt/C (54 mV dec^{-1}), Co_2P @ NC (116 mV dec^{-1}), Mo_2C@NC (153 mV dec^{-1}), and CP (241 mV dec^{-1}). Tafel slopes of 120, 40, and 30 mV dec^{-1} correspond to the Volmer, Heyrovsky, and Tafel processes, respectively, suggesting that the reaction

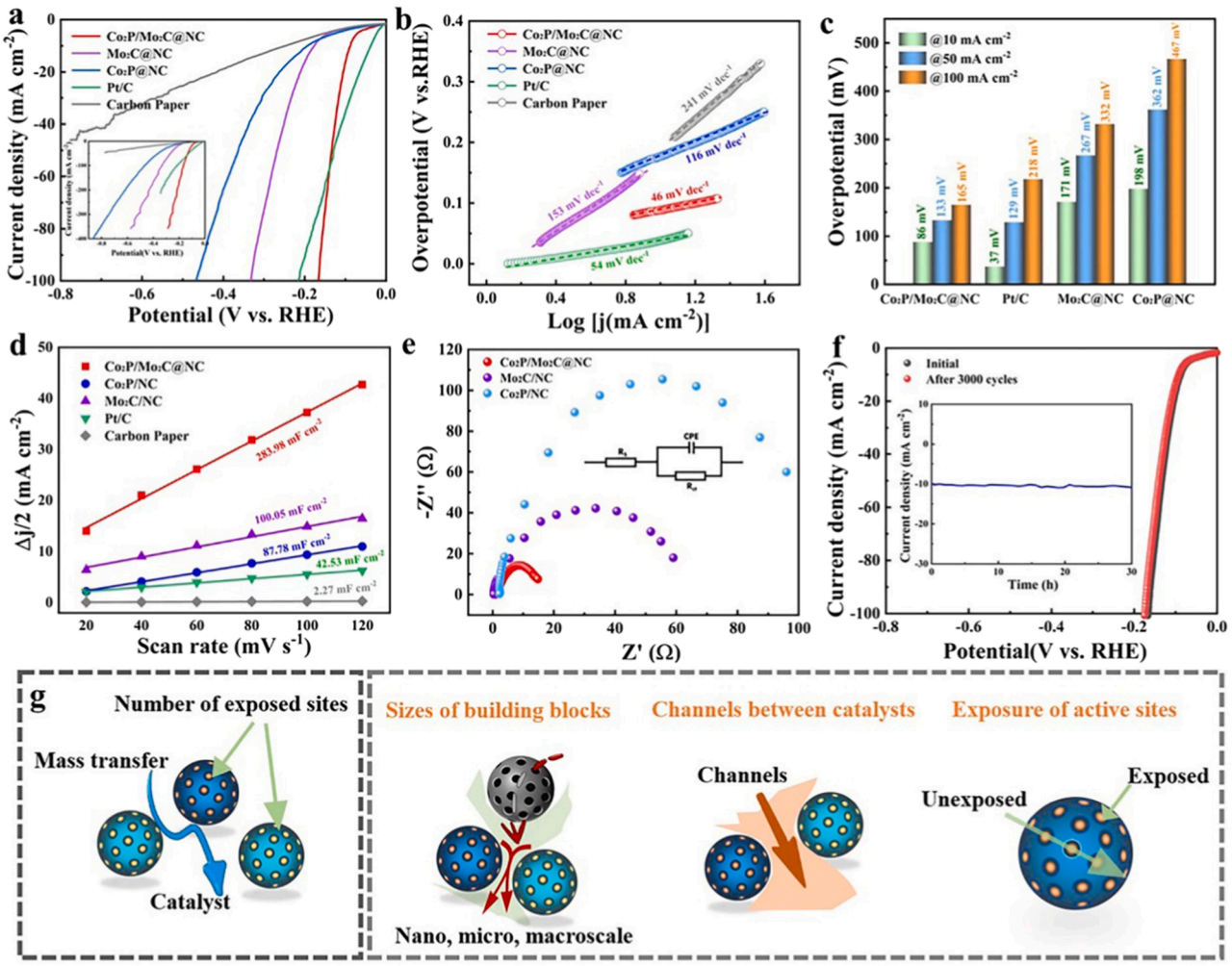

Fig. 3. (a) LSV curves of Co_2P/Mo_2C@NC, Mo_2C@NC, Co_2P @ NC, carbon paper, and Pt/C for HER in 1 M KOH at a scanning rate of 5 mV s^{-1}. (b) Tafel plots of all studied electrocatalysts. (c) Bar plots of overpotentials to drive current densities of 10, 50, and 100 mA cm^{-2} of the prepared nanomaterials. (d) Relationships between capacitive current densities (Δj) measured on Co_2P/Mo_2C@NC, Mo_2C@NC, Co_2P @ NC, carbon paper, and Pt/C electrocatalysts against different scan rates in 1.0 M KOH. (e) EIS Nyquist plots of different catalysts. Inset shows the equivalent circuit, R_s: external resistance, *CPE*: constant phase element, and R_{ct}: electrochemical charge transfer resistance. (f) Polarization curves of Co_2P/Mo_2C@NC before and after stability testing for 3000 cycles. Inset: the chronoamperometry curve of Co_2P/Mo_2C@NC recorded for 30 h at −10 mA cm^{-2}. (g) Schematics showing key aspects of the design of catalysts for Co_2P/Mo_2C@NC water splitting.

proceeds through the Volmer–Heyrovsky mechanism [8,40]. The Tafel slope of Co_2P/Mo_2C@NC was 46 mV dec^{-1}, indicating that the HER pathway followed the Volmer–Tafel mechanism. Moreover, the interfacial properties of the electrode/electrolyte were studied using EIS, to gain further insights to the kinetics of the electrode reaction. Nyquist curves of representative Co_2P/Mo_2C@NC, Co_2P @ NC, and Mo_2C@NC samples are shown in Fig. 3e. The illustration shows the equivalent circuit model of the electrochemical impedance test. From the radius of the semicircle at the high frequency region, it can be presumed that the electron transfer resistance (R_{ct}) represents the charge transfer resistance between the catalyst surface and the electrolyte. The results show that Co_2P/Mo_2C@NC has the shortest semicircle, fastest electron transfer rate, and the fastest kinetics.

It is well known that an increase in the electrochemically active surface area (ECSA) accelerates the catalytic activity of the electrode. The high activity of the Co_2P/Mo_2C@NC electrode was confirmed by an ECSA calculation [40]. The ECSA of the catalyst was estimated using the following formula: [41] ECSA $= \frac{C_{dl}}{C_s}$, where Cs is the specific capacitance in an alkaline electrolyte (Cs = 0.040 mF cm^{-2}), and C_{dl} is the electrochemical double-layer capacitance. The ECSA was proportional to the electrochemical double-layer capacitance (C_{dl}). C_{dl} was measured using CV. CV measurements were carried out in a 1 M KOH solution at different scan rates (20, 40, 60, 80, 100, and 120 mV s^{-1}) for all samples (Fig. S1). Fig. S1 shows that Co_2P/Mo_2C@NC has a higher peak potential separation and larger peak current density than those of Co_2P @ NC and Mo_2C@NC, indicating a larger electroactive surface area and faster electron transfer. The increase in the peak current density indicated the enhanced electrocatalytic activity of Co_2P/Mo_2C@NC. C_{dl} is derived from the slope of the linear relationship between the current density and scan rate. In particular, as shown in Fig. 3d, the C_{dl} of Co_2P/Mo_2C@NC is 283.98 mF cm^{-2}. It is much larger than those of Pt/C (42.53 mF cm^{-2}), Co_2P @ NC (87.78 mF cm^{-2}), Mo_2C@NC (100.05 mF cm^{-2}) and the naked CP (2.27 mF cm^{-2}), which reveals the more easily available active sites in Co_2P/Mo_2C@NC. The results revealed that the heterojunction interface formed between Co_2P and Mo_2C nanoparticles enhanced the synergistic effect between them and provided the best HER activity. The intrinsic catalytic activity of the catalyst may be a fundamental factor in improving the water splitting performance [42].

Electrochemical stability is another key factor affecting the practical application of electrocatalysts. To evaluate the long-term stability, a CV scanning test was performed at 100 mV s^{-1}, and negligible attenuation was observed in the polarization curve of Co_2P/Mo_2C@NC after 3000 CV cycles (Fig. 3f). In addition, the Co_2P/Mo_2C@NC chronoamperometry measurements at 10 mA cm^{-2} show negligible current density loss after 30 h of continuous operation, indicating outstanding HER stability (inset in Fig. 3f). The SEM images of the Co_2P/Mo_2C@NC samples after the HER showed that the morphology remained intact after the stability test (Fig. S2c), indicating the structural stability of Co_2P/Mo_2C@NC.

The above results show that the improvement in the activity of the catalyst can be attributed to the decrease in the charge transfer resistance of the N-doped porous C-supported Co_2P/Mo_2C-heterojunction, increase in the number of active sites, and enhancement of the intrinsic catalytic activity. The nano-, micro-, and macro-scale structures of the porous catalyst jointly determine the size of the channels and the exposure of the active sites to the electrolyte (Fig. 3**g**). This is also an aspect that can be engineered towards better high current density performance for water splitting by (1) increasing the mass transfer ability and (2) increasing the number of active sites for catalysis [43].

3.3. Electrocatalytic performances of Co_2P/Mo_2C@NC toward OER

The electrocatalytic OER performance was evaluated in N_2 saturated 1.0 M KOH at a scanning rate of 5 mV s^{-1}. In the same electrolyte, Co_2P/Mo_2C@NC exhibited excellent HER and OER activities. As expected from the polarization curves of the representative samples, the performance of Co_2P/Mo_2C@NC was better than that of commercial RuO_2 (Fig. 4a and c). The overpotential of Co_2P/Mo_2C@NC is the smallest; $\eta(10)$ is 209 mV; $\eta(50)$ is 270 mV; $\eta(100)$ is 350 mV. Its $\eta(10)$ is 31 mV lower than that of RuO_2 ($\eta 10 = 240$ mV) and much lower than that of Co_2P @ NC ($\eta 10 = 301$ mV). Notably, the overpotential of Mo_2C@NC ($\eta 10 = 181$ mV) was lower than that of Co_2P/Mo_2C@NC ($\eta 10 = 209$ mV); however, the overpotential tended to increase when the current density was above 13 mA cm^{-2} (Fig. 4a). The Tafel slope of Co_2P/Mo_2C@NC is 91 mV dec^{-1}, which is lower than those of RuO_2 (132 mV dec^{-1}), Mo_2C@NC (140 mV dec^{-1}), and Co_2P @ NC (169 mV dec^{-1}) (Fig. 4b), indicating the faster OER dynamics of Co_2P/Mo_2C@NC. In general, the OER involves four electron transfer steps, with one electron transferred in each step. The energy barrier for each step leads to sluggish kinetics in the OER process [44]. A Tafel slope of 40 mV dec^{-1} suggests that the step involving two-electron transfer is the RDS, and a Tafel slope near 60 mV dec^{-1} is associated with a rate-limiting step that follows the first electron transfer [45].

The low overpotential and small Tafel slope of the Co_2P/Mo_2C@NC electrode are comparable to those of other OER catalysts reported in the literature (Table S2), indicating its high OER activity. As shown in Fig. 4**e**, the R_{ct} of Co_2P/Mo_2C@NC was significantly lower than those of RuO_2, Mo_2C@NC, Co_2P @ NC, and the naked CP, which indicates its fast electron transport and improved electrochemical kinetics owing to interfacial electron redistribution. In addition, to further explore the reason for the increase in the intrinsic activity of the electrocatalyst, the ECSA was measured (Fig. 4d). The ECSA is a reflection of the surface area of the catalyst that can be catalyzed and is proportional to the double-layer capacitance (C_{dl}) [46]. The C_{dl} values were measured using CV at different scanning rates in the non-Faraday potential range (Fig. S4), which was used to estimate the ECSA. Compared with Mo_2C@NC (6.74 mF cm^{-2}), Co_2P @ NC (54.41 mF cm^{-2}), and RuO_2 (22.49 mF cm^{-2}), Co_2P/Mo_2C@NC had the highest C_{dl} of 133.35 mF cm^{-2}, indicating the highest ECSA. The highest ECSA values indicate that the Co_2P/Mo_2C@NC has a higher electrochemical surface area, which enhances the OER performance. In addition to catalytic activity, we tested the stability of the Co_2P/Mo_2C@NC catalyst at a current density of 10 mA cm^{-1} for 30 h. As illustrated in Fig. 4f, the Co_2P/Mo_2C@NC electrode maintained its initial activity during the 30 h continuous chronopotentiometric electrolysis with insignificant loss. Fig. 4f shows a negligible change in the polarization curve for the OER before and after the stability test, indicating that the OER demonstrates an extremely high durability. The morphology and Crystallinity of the Co_2P/Mo_2C@NC samples after the OER was characterized using SEM and XRD. After cyclic testing, the morphology of the porous structure remained good, and the crystallinity did not change, further confirming the structural stability of the Co_2P/Mo_2C@NC catalyst for the OER (Fig. S2d and Fig. S3).

3.4. Evaluation of the electrocatalytic overall water splitting performance

Considering the excellent performance of the Co_2P/Mo_2C@NC catalyst for HER and OER in an alkaline medium, a water–alkali electrolytic cell with a double electrode structure was assembled by using it as a bifunctional catalyst. The entire water-splitting experiment was performed with Co_2P/Mo_2C@NC as the anode and cathode. As shown in Fig. 5a, in a two-electrode system, electrons can pass rapidly through a porous catalyst supported on CP because its high conductivity can dissociate H_2O and OH^- adsorbed on Co_2P/Mo_2C@NC and generate H_2 at the cathode and O_2 at the anode, respectively. As expected, the Co_2P/Mo_2C@NC pair significantly outperformed the Pt/C||RuO_2 pair. Co_2P/Mo_2C@NC shows excellent catalytic activity for overall water decomposition, providing a current density of 10 mA cm^{-2} at only 1.55 V, which is much lower than that of Pt/C||RuO_2 (1.62 V). Significantly, the electrochemical performance of the Co_2P/Mo_2C@NC pair in a 1.0 M KOH electrolyte was also superior to that of previous platinum-group

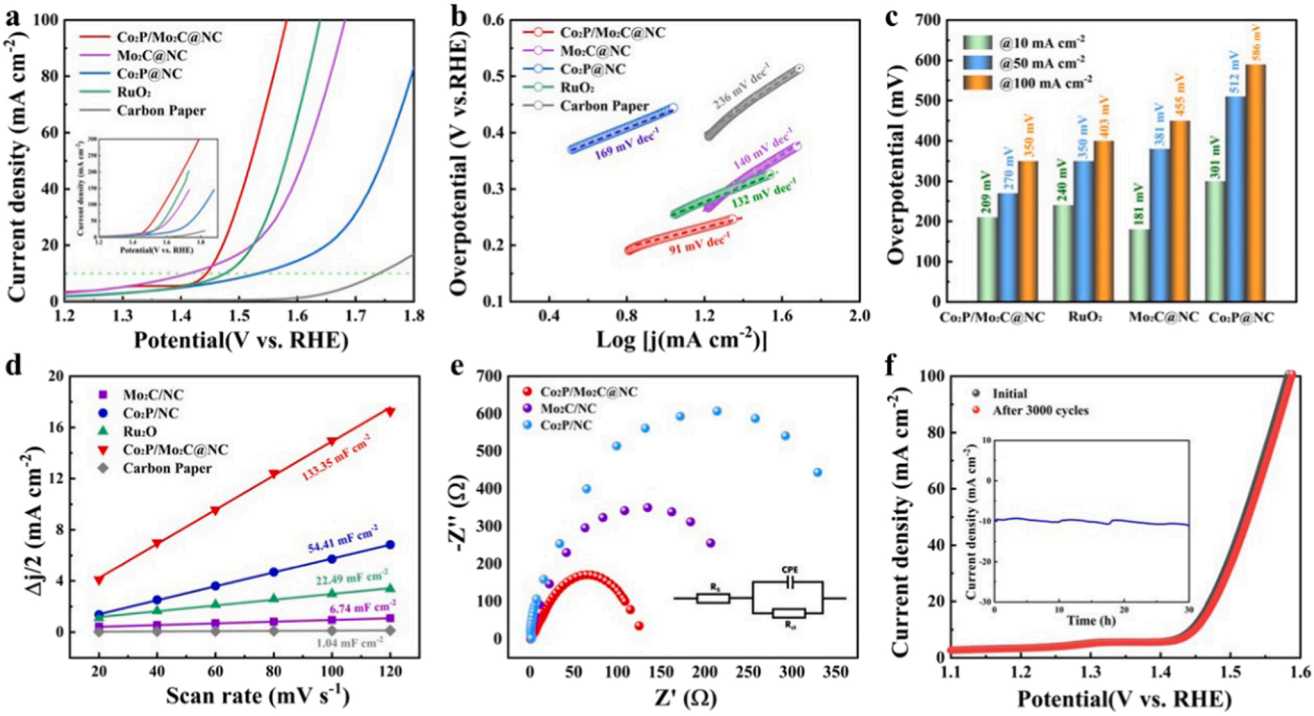

Fig. 4. (a) OER LSV curves in 1 M KOH at a scan rate of 5 mV s^{-1} and (b) corresponding Tafel slopes. (c) Corresponding overpotentials at $j = 10$, 50, and 100 mA cm^{-2}. (d) Charging current–density difference plotted against the scan rate to yield the C_{dl} of the catalysts and (e) Nyquist plots with a potential of + 1.535 V vs. RHE. (f) Polarization curve of Co_2P/Mo_2C@NC after 3000 continuous cycles at 100 mV s^{-1} (inset: chronoamperometric curve at $\eta = 10$ mV for OER catalyzed by Co_2P/Mo_2C@NC for the stability test).

metal electrocatalysts, such as RuO_2/Co_3O_4 [47] and Pt-CoS_2 /CC [48] (Fig. 5h). In addition, the Faraday efficiency (FE) of Co_2P/Mo_2C@NC in an H-type electrolysis device was evaluated by comparing the actual and theoretical gas productions of the catalyst (Fig. 5b and c). The theoretical gas production is consistent with that measured, with FE approaching 100% for the HER and OER. In addition, the Co_2P/-Mo_2C@NC chronopotentiometric curves at 10 mA cm^{-2}, 50 mA cm^{-2}, and 100 mA cm^{-2} current densities demonstrate good long-term stability (Fig. 5d). The low overpotential and good stability of Co_2P/-Mo_2C@NC make it one of the best bifunctional electrocatalysts. Therefore, even the 1.55 V solar cell voltage can drive the Co_2P/-Mo_2C@NC pairs to produce significant bubbles, which shows its potential for solar storage and actual hydrogen production (Fig. 5f and g). In addition, the *J–V* curve of the series solar cell intersects the *J–V* curve of the electrolyzer, and the expected working current density of the photoelectrolysis system at 1.78 V is 14.7 mA cm^{-2} (Fig. 5e). We further characterized the performance of the combined system under a light irradiation of AM 1.5 G 100 mW cm^{-2}. The system achieved a stable STH conversion efficiency of 18.1% (see the detailed calculation in the experimental process), demonstrating the application potential of Co_2P/Mo_2C@NC in an actual photo-driven water splitting system.

3.5. Theoretical calculations and mechanism analysis

To gain insights into the heterointerface effects on significantly enhanced catalytic activities, we then performed DFT calculations. The specific calculation method is described in the Experimental Section. The optimized atomic models of Co_2P, Mo_2C, Co_2P/Mo_2C heterojunction, and Co_2P/Mo_2C@NC are displayed in Fig. S5 (Supporting Information). As shown in Fig. 6 (a-d), the projected density of states (PDOS) displays that the Co orbital of Co_2P/Mo_2C and Co_2P/Mo_2C@NC have a higher density state near the Fermi level than the Co orbital of Co_2P and Mo orbital of Mo_2C, indicating the remarkably enhanced electron transfer conferred by the construction of Co_2P/Mo_2C heterogeneous interface. This observation was also consistent with the EIS analysis (Fig. 3e), corroborating the enhanced electrocatalytic properties.

In order to microscopically understand the better electron transfer on the Co_2P/Mo_2C@NC, we firstly analyze the charge transfer at the Co_2P/Mo_2C@NC heterogeneous interface by calculating the charge density difference, which is given in Fig. 7(d). It can be clearly observed that, due to the van der Waals interaction at the interface, the charge transfer is mainly concentrated at the interface of Co_2P/Mo_2C heterostructures. The electrons enter the Co_2P layer from Mo_2C and accumulate on the Co_2P surface, holes accumulate on the surface of Mo_2C layer. We then use bader charge analysis to calculate the number of electrons transfer (Supplementary Table S3). Compared to the Co_2P and Mo_2C, the higher bader charge on the Co active site in Co_2P/Mo_2C and Co_2P/Mo_2C@NC indicates its stronger oxidation capacity as well as more beneficial electron transfer Fig. 6(f). The calculated results also show that the electrons transfer from Mo to Co is about 0.21|e|, indicating to agree with the charge density difference. In sum, the calculated electron density distribution proves that the electron transfer occurs at the interface between Co_2P and Mo_2C, and electrons move from Mo to Co. The free energy diagrams of OER over Co_2P, Mo_2C, Co_2P/Mo_2C, and Co_2P/Mo_2C@NC (Fig. 6e and Supplementary Table S4) reveals that the free energy of Co_2P changes for the four steps are + 0.71, + 1.41, + 2.12, and + 0.58 eV, respectively; therefore, the rate-determining step (RDS) is the third step. By contrast, for Co_2P/Mo_2C@NC, the free energy changes for the four steps are + 0.55, + 1.14, + 2.02, and + 1.21 eV, respectively. The RDS is the third step; also, the lower energy change for the RDS (+2.02 eV) implies that the Co_2P/Mo_2C@NC heterojunction could promote the OER kinetics. Generally, the Gibbs free energy of hydrogen adsorption (ΔG_{H^*}) is used to evaluate the HER catalytic performance of the prepared catalyst. Theoretically, ΔG_{H^*} with an absolute value close to 0 eV enables preferable H adsorption and desorption strength. The water adsorption/desorption and the adsorption/desorption of H are the key descriptors for the HER under alkaline

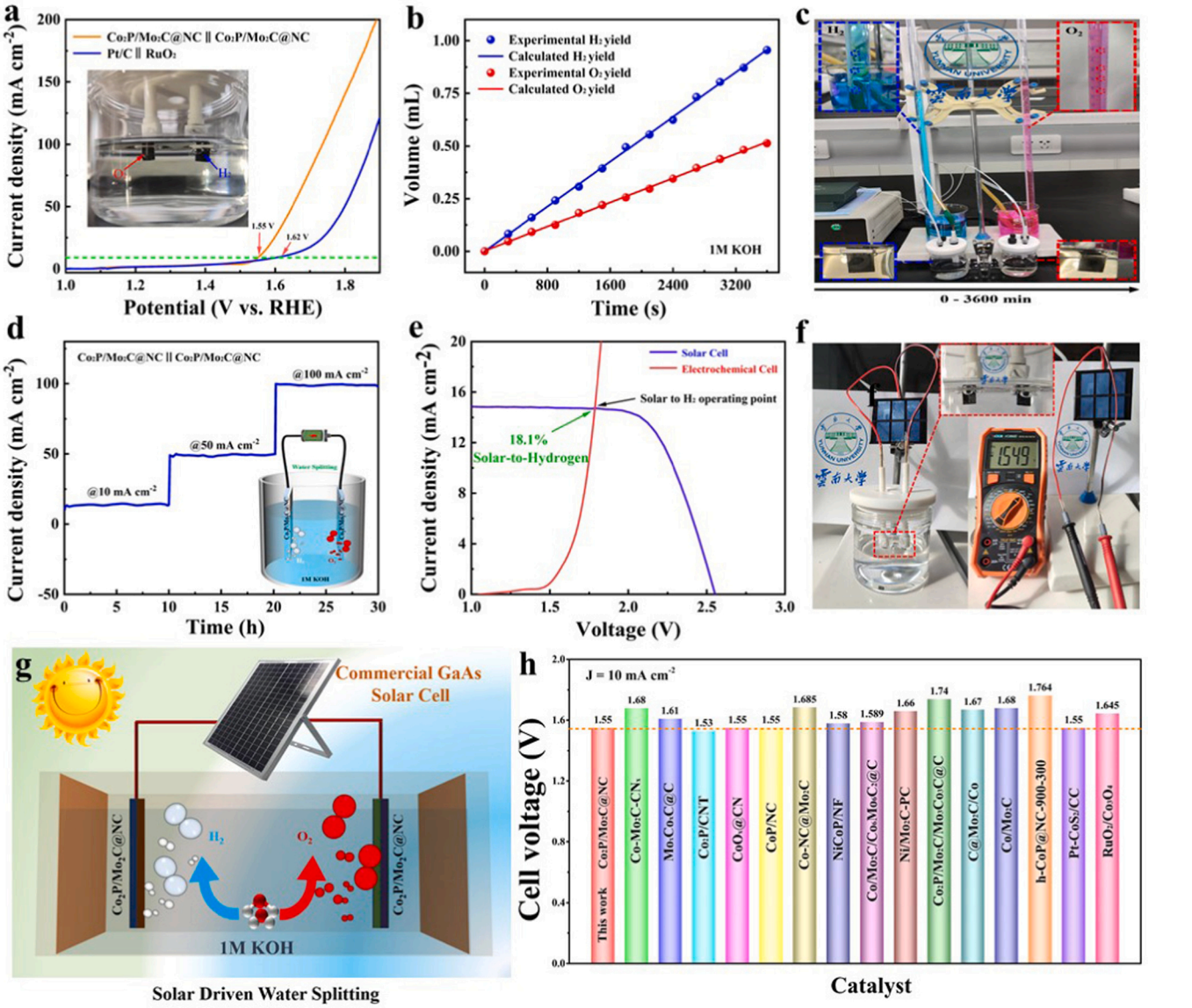

Fig. 5. Water splitting performance of Co_2P/Mo_2C@NC. (a) Two-electrode polarization curves of Co_2P/Mo_2C@NC//Co_2P/Mo_2C@NC and Pt/C//RuO_2 for water splitting in 1 M KOH with 85% iR-correction. Inset of (a) showing the Co_2P/Mo_2C@NC electrolyzer unit. (b) FE of Co_2P/Mo_2C@NC for overall water splitting at a constant current density of 100 mA cm^{-2}. (c) Digital photograph of the electrolytic water splitting gas collection device. (d) Stability measurement using the V–t curve of Co_2P/Mo_2C@NC recorded for 30 h at 10, 50, and 100 mA cm^{-2}. (e) *J–V* curves under simulated AM 1.5 G 100 mW cm^{-2} illumination for a GaAs cell integrated with the overall water splitting system. (f) Digital photograph of the water electrolyzer driven by a 1.55 V solar cell. (g) Schematic of the photo-driven water splitting system. (h) Cell voltages of different electrolyzers constructed by bifunctional electrocatalysts for water electrolysis, Electrolyte is 1.0 M KOH (Table S2, Supporting Information).

conditions. As displayed in Fig. 7c, the negative water adsorption energies for Co_2P, Mo_2C, Co_2P/Mo_2C, and Co_2P/Mo_2C@CN were investigated, indicating that adsorption energies of both Co_2P/Mo_2C and Co_2P/Mo_2C@CNP are favorable for water adsorption compared with that of Mo_2C. Compared with Co_2P and Mo_2C, the Co_2P/Mo_2C heterojunction showed a much lower adsorption energy of H_2O (ΔG_{H2O}*), indicating the strongest water adsorption. This benefits the subsequent step in generating adsorbed HO–H atoms. Subsequently, the free-energy diagrams of the HER for different Co sites on the Co_2P and Co_2P/Mo_2C heterojunction and Mo sites on the Mo_2C and Co_2P/Mo_2C heterojunctions (Fig. 6f) were investigated, indicating that the Co in the Co_2P/Mo_2C heterojunction features the lowest energy change (absolute value of 0.203 eV). Therefore, for both the OER and HER, the effect of the Co_2P/Mo_2C heterojunction played a crucial role in optimizing the reaction kinetics.

To investigate the stability, we examined the catalyst after HER tests. As shown in Fig. S7, XPS shows that the Mo2p and Co2p peaks shift considerably after the HER stability test, and the intensities of the Mo^{2+} and $Co^{\delta+}$ ($O < \delta < 2$) peaks in Mo2p and Co2p decrease, indicating that Mo and Co atoms are further oxidized in the HER process. When atoms combine into molecules or crystals, the valence electrons are transferred or shared, and this charge change in the valence electrons leads to a change in the binding energy of the inner electrons. In all these cases, the isolated metal center with a slight positive charge acted as the hydride receptor site. For the nanostructure Co_2P, the binding energies of P (129.8 eV) and Co (779.3 eV) are very close to those of the corresponding zero-valent species P (128.5 eV) and Co (778.2 eV), indicating that P and Co are the receptor centers of protons and hydrides, respectively. Similar results have been reported in the literature [23]. Further, HR XPS (Fig. S7b) of P2p shows a wide peak centered at 131.5 eV, corresponding to PO_4^{2-}, whereas the characteristic peak of the original phosphide disappears completely at 133.3 eV [49]. These observations

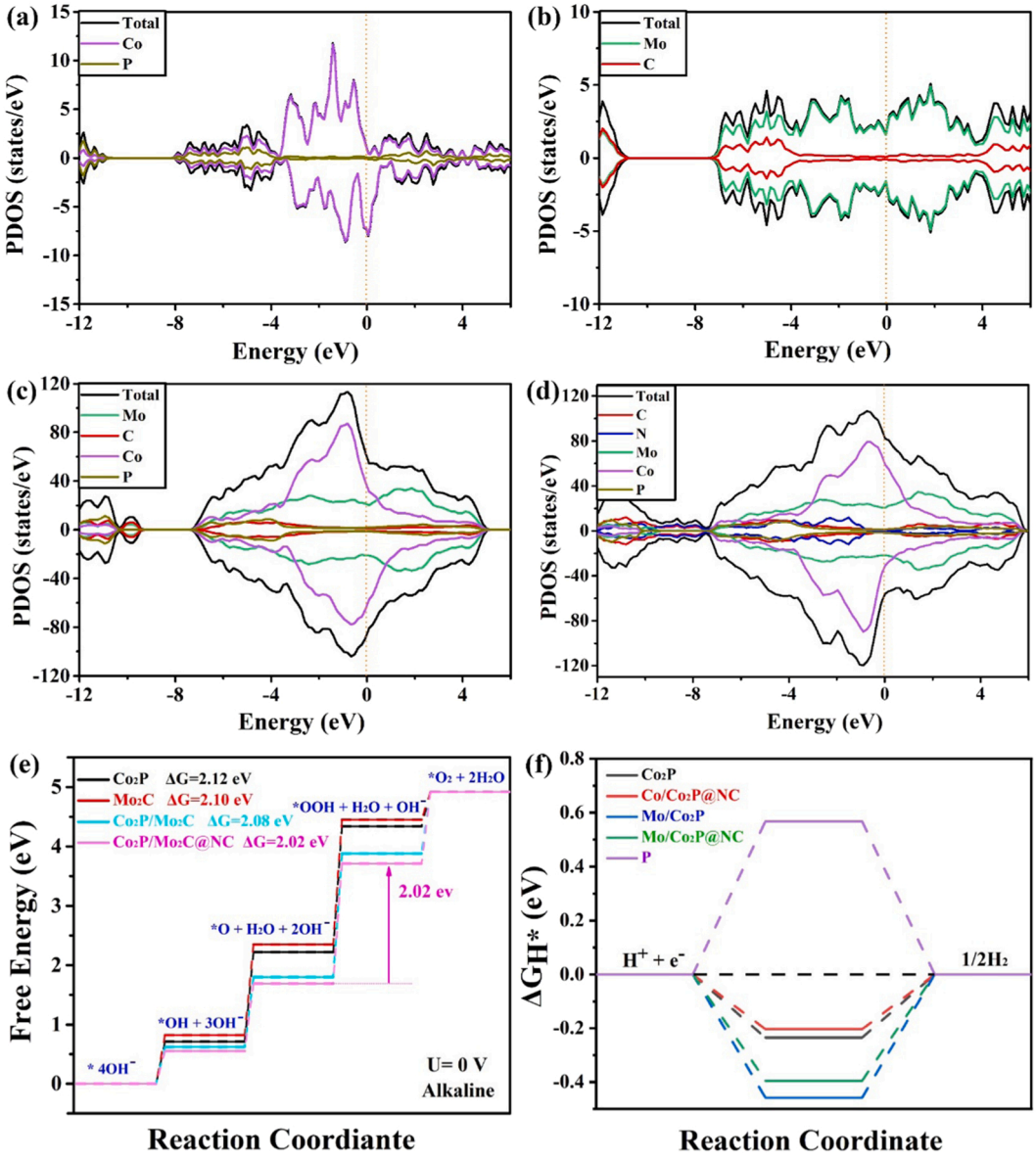

Fig. 6. Theoretical calculation analysis. (a-b) Calculated PDOS in the four compounds. Free energy diagrams of the Co_2P, Mo_2C, Co_2P/Mo_2C, and Co_2P/Mo_2C@NC models for (e) OER, and (f) HER, respectively.

suggest that the initial Co_2P/Mo_2C@NC catalysts are partially oxidized to cobalt oxides/hydroxides and cobalt phosphate, which may then act as effective HER and OER catalysts in conjunction with Co_2P. This observation is consistent with the findings of recent studies on CoP [50] and Ni_2P [21] electrocatalysts with metal phosphide cores and corresponding metal oxide/hydroxide shells.

Considering the above analytical results, the excellent activity of the coupled nitrogen-doped carbon-wrapped Co_2P/Mo_2C heterogeneous catalyst toward overall water splitting can be explained as follows: (i) The coexistence of Co_2P and Mo_2C increases the affinity between them and promotes the water cracking reaction. The Co_2P center can promote H adsorption, whereas nearby Mo_2C species preferentially adsorb OH^- from water decomposition, thereby completing the Volmer–Heyrovsky process. In addition, the introduction of Co_2P significantly increased the activity of Mo_2C while also increasing the number of defects or edge locations in the Mo_2C structure, facilitating the proton-coupled electron transfer step. (ii) The existence of interface charge regulation driven by the Mott–Schottky effect between semiconductors Co_2P and Mo_2C. The electrons in the transition metal can be transferred to Mo and occupy its d orbital. This increases the d orbital occupation of Mo in Mo_2C to obtain a suitable Mo–H bond energy, thereby providing excellent adsorption and desorption properties suitable for splitting water. (iii) The carbon matrix and N and P heteroatom co-doping in Co_2P/Mo_2C@NC contributed significantly to the excellent electrocatalytic performance of the catalyst. Doping heteroatoms in carbon materials, whether dopants with a higher or lower electronegativity than carbon, will destroy the electron neutrality of carbon and induce charge redistribution, resulting in more active centers. In particular, the double doping of heteroatoms, such as N (3.04) and P (2.19), which are opposite to C (3.16), can produce significant carbon electron donor properties through synergistic coupling between the two heteroatoms, thereby substantially improving the electrocatalytic activity of the catalyst. (iv) The 3D porous honeycomb carbon network structure not only exposes and better utilizes the active center but also enriches the electron/ion diffusion pathway and accelerates the charge transfer speed of the electrocatalyst. This also allows the electrolyte to enter completely and provides a large number of additional heterogeneous catalytic sites that are exposed to the surface of the catalyst. (v) DFT calculations confirmed that Co_2P coupled

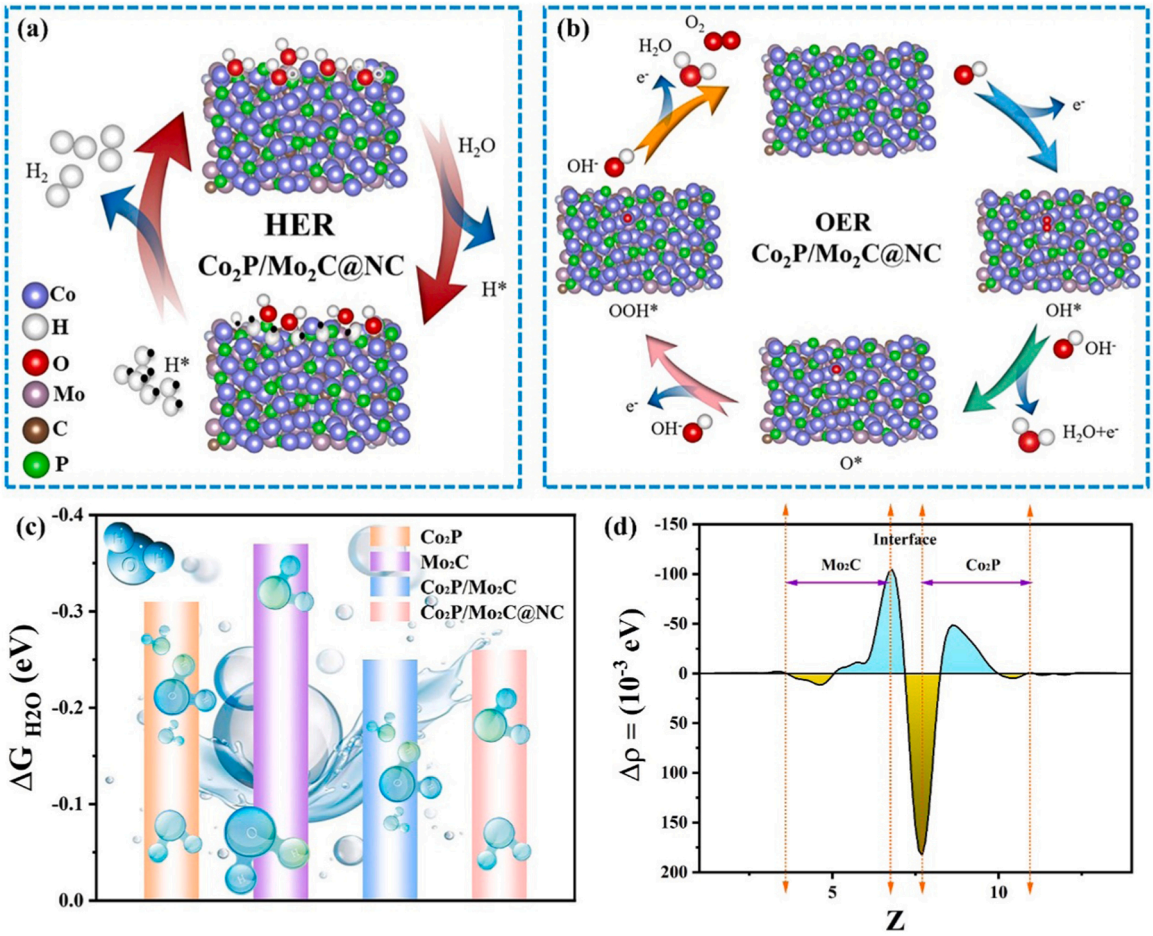

Fig. 7. Theoretical calculation analysis. (a-b) Models of adsorption configuration of OER, and HER on Co_2P/Mo_2C@NC heterojunction catalyst. Purple balls = Co, pink balls = Mo, red balls = C, green balls = P, white balls = H, and red balls = O. (c) Calculated adsorption free energy of water on Co_2P, Mo_2C, Co_2P/Mo_2C, and Co_2P/Mo_2C@NC surfaces. (d) Plane-averaged electrostatic potential drop across the interface of the Co_2P/Mo_2C@NC.

with Mo_2C in Co_2P/Mo_2C@NC could optimize the ΔG_{H^*} and ΔE_{H2O}, accelerating catalytic kinetics and thereby boosting the overall water splitting performance.

4. Conclusion

In summary, the coupling of Co, Mo, P, C and N was realized via one-step pyrolysis in a limited space, and a honeycomb-like porous Co_2P/Mo_2C@NC nanostructure was obtained. Owing to the unique heterostructure and synergistic effect of Mo_2C and Co_2P, the Co_2P/Mo_2C@NC catalysts exhibited excellent hydrogen and oxygen evolution performance. Notably, the electrode exhibited an excellent bifunctional catalytic activity. In an alkaline medium, overpotentials of only 86 mV and 209 mV can provide a current density of 10 mA cm^{-2} for the HER and OER, respectively. It was revealed experimentally and theoretically that this impressive water splitting performance can be attributed to the introduction of the Co_2P impurity phase, which can obtain an appropriate Mo–H bond energy through the direct interface interaction between the Co_2P impurity phase and Mo_2C, thereby providing excellent adsorption and desorption properties for water splitting. In addition, heteroatom doping improves the activity of the catalyst; the 3D porous morphology increases the contact area between the catalyst and the electrolyte and increases the number of active centers, and the heterostructure realizes interfacial charge regulation driven by the Mott–-Schottky effect. In conclusion, the synergistic regulation of heteroatomic heterostructures and electronic structures is an effective way to improve the number and intrinsic activity of the water-splitting active sites. This provides inspiration for the rational design of non-precious metal-based materials to achieve the efficient conversion of electrochemical energy. In addition, this study can generate electricity and store excess electricity through solar cells, and use hydrogen as energy storage medium, which is expected to solve the limitations of traditional "dependent on the weather" photovoltaic hydrogen production and the electrolytic water hydrogen production consumption of a large amount of electric energy, thereby facilitating energy conservation and achieving a low-carbon economy.

CRediT authorship contribution statement

Pengliang Sun: Conceptualization, Methodology, Investigation, Data curation, Writing – original draft. **Yingtang Zhou:** DFT calculation, Check draft, Investigation, Visualization. **Hongyi Li:** Validation, Investigation, Software. **Hua Zhang:** Data curation, Physicochemical characterization. **Ligang Feng:** Visualization, Resources, Writing – review & editing. **Qiue Cao:** Visualization, Investigation. **Shixi Liu:** Supervision, Funding acquisition, Writing – review & editing. **Thomas Wågberg:** Investigation, Funding acquisition. **Guangzhi Hu:** Supervision, Funding acquisition, Writing – review & editing.

Declaration of Competing Interest

The authors declare that they have no known competing financial interests or personal relationships that could have appeared to influence the work reported in this paper.

Acknowledgements

The authors acknowledge the financial support by the National Natural Science Foundation of China (U2002213, 22164020), the Double Tops Joint Fund of the Yunnan Science and Technology Bureau and Yunnan University (2019FY003025), 'Double First Class' University Construction Project (C176220100042). T.W. acknowledges the support from Vetenskapsrådet (2017-04862 and 2021-04629), Energimyndigheten (45419-1), and SSF-Agenda 2030-PUSH. The authors thank the Advanced Analysis and Measurement Center of Yunnan University for the sample testing service.

Appendix A. Supporting information

Supplementary data associated with this article can be found in the online version at doi:10.1016/j.apcatb.2022.121354.

References

[1] B.Y. Xia, Y. Yan, N. Li, H.B. Wu, X.W. Lou, X. Wang, A metal–organic framework-derived bifunctional oxygen electrocatalyst, Nat. Energy 1 (2016) 1–8.
[2] P. Zhai, M. Xia, Y. Wu, G. Zhang, J. Gao, B. Zhang, S. Cao, Y. Zhang, Z. Li, Z. Fan, C. Wang, X. Zhang, J.T. Miller, L. Sun, J. Hou, Engineering single-atomic ruthenium catalytic sites on defective nickel-iron layered double hydroxide for overall water splitting, Nat. Commun. 12 (2021) 1–11.
[3] Y. Chen, B. Gao, M. Wang, X. Xiao, A. Lv, S. Jiao, P.K. Chu, Dual-phase MoC-Mo_2C nanosheets prepared by molten salt electrochemical conversion of CO_2 as excellent electrocatalysts for the hydrogen evolution reaction, Nano Energy 90 (2021), 106533.
[4] R. Zhang, Z. Wei, G. Ye, G. Chen, J. Miao, X. Zhou, X. Zhu, X. Cao, X. Sun, *d*-electron complementation induced V-Co phosphide for efficient overall water splitting, Adv. Energy Mater. 11 (2021) 2101758.
[5] Y. Jiao, Y. Zheng, K. Davey, S.-Z. Qiao, Activity origin and catalyst design principles for electrocatalytic hydrogen evolution on heteroatom-doped graphene, Nat. Energy 1 (2016) 1–9.
[6] S. Li, Z. Zhao, T. Ma, P. Pachfule, A. Thomas, Superstructures of organic-polyoxometalate co-crystals as precursors for hydrogen evolution electrocatalysts, Angew. Chem. Int. Ed. Engl. 134 (2021), e202112298.
[7] L. Deng, K. Zhang, D. Shi, S. Liu, D. Xu, Y. Shao, J. Shen, Y. Wu, X. Hao, Rational design of Schottky heterojunction with modulating surface electron density for high-performance overall water splitting, Appl. Catal. B Environ. 299 (2021), 120660.
[8] H. Zhang, H. Li, S. Niu, Y. Zhou, Z. Ni, Q. Wei, A. Chen, S. Zhang, T. Sun, R. Dai, Y. Yang, G. Hu, Bifunctional heterostructured nitrogen and phosphorus co-doped carbon-layer-encapsulated Co_2P electrocatalyst for efficient water splitting, Cell Rep. Phys. Sci. 2 (2021), 100586.
[9] D. Chen, Z. Pu, R. Lu, P. Ji, P. Wang, J. Zhu, C. Lin, H.W. Li, X. Zhou, Z. Hu, F. Xia, J. Wu, S. Mu, Ultralow Ru loading transition metal phosphides as high-efficient bifunctional electrocatalyst for a solar-to-hydrogen generation system, Adv. Energy Mater. 10 (2020) 2000814.
[10] Z. Wu, Y. Zhao, H. Wu, Y. Gao, Z. Chen, W. Jin, J. Wang, T. Ma, L. Wang, Corrosion engineering on iron foam toward efficiently electrocatalytic overall water splitting powered by sustainable energy, Adv. Funct. Mater. 31 (2021) 2010437.
[11] H. Yang, M. Driess, P.W. Menezes, Self-supported electrocatalysts for practical water electrolysis, Adv. Energy Mater. 11 (2021) 2102074.
[12] K. Hu, T. Ohto, Y. Nagata, M. Wakisaka, Y. Aoki, J.I. Fujita, Y. Ito, Catalytic activity of graphene-covered non-noble metals governed by proton penetration in electrochemical hydrogen evolution reaction, Nat. Commun. 12 (2021) 1–9.
[13] K. Wang, Y. Guo, Z. Chen, D. Wu, S. Zhang, B. Yang, J. Zhang, Regulating electronic structure of two-dimensional porous Ni/Ni_3N nanosheets architecture by Co atomic incorporation boosts alkaline water splitting, InfoMat (2021).
[14] Q. Gao, W. Zhang, Z. Shi, L. Yang, Y. Tang, Structural design and electronic modulation of transition-metal-carbide electrocatalysts toward efficient hydrogen evolution, Adv. Mater. 31 (2019) 1802880.
[15] L. He, W. Zhang, Q. Mo, W. Huang, L. Yang, Q. Gao, Molybdenum carbide-oxide heterostructures: in situ surface reconfiguration toward efficient electrocatalytic hydrogen evolution, Angew. Chem. Int. Ed. Engl. 132 (2020) 3572–3576.
[16] W. Li, C. Wang, X. Lu, Integrated transition metal and compounds with carbon nanomaterials for electrochemical water splitting, J. Mater. Chem. A 9 (2021) 3786–3827.
[17] Q. Liu, J. Tian, W. Cui, P. Jiang, N. Cheng, A.M. Asiri, X. Sun, Carbon nanotubes decorated with CoP nanocrystals: a highly active non-noble-metal nanohybrid electrocatalyst for hydrogen evolution, Angew. Chem. Int. Ed. Engl. 53 (2014) 6710–6714.
[18] X.W. Lv, W.S. Xu, W.W. Tian, H.Y. Wang, Z.Y. Yuan, Activity promotion of core and shell in multifunctional core-shell Co_2P@NC electrocatalyst by secondary metal doping for water electrolysis and Zn-air batteries, Small 17 (2021) 2101856.
[19] J. Li, C. Zhang, H. Ma, T. Wang, Z. Guo, Y. Yang, Y. Wang, H. Ma, Modulating interfacial charge distribution of single atoms confined in molybdenum phosphosulfide heterostructures for high efficiency hydrogen evolution, Chem. Eng. J. 414 (2021), 128834.
[20] H. Wang, H. Zou, Y. Liu, Z. Liu, W. Sun, K.A. Lin, T. Li, S. Luo, Ni_2P nanocrystals embedded Ni-MOF nanosheets supported on nickel foam as bifunctional electrocatalyst for urea electrolysis, Sci. Rep. 11 (2021) 1–11.
[21] F. Yu, H. Zhou, Y. Huang, J. Sun, F. Qin, J. Bao, W.A. Goddard 3rd, S. Chen, Z. Ren, High-performance bifunctional porous non-noble metal phosphide catalyst for overall water splitting, Nat. Commun. 9 (2018) 1–9.
[22] H. Pei, L. Zhang, G. Zhi, D. Kong, Y. Wang, S. Huang, J. Zang, T. Xu, H. Wang, X. Li, Rational construction of hierarchical porous FeP nanorod arrays encapsulated in polypyrrole for efficient and durable hydrogen evolution reaction, Chem. Eng. J. (2021), 133643.
[23] D. Das, K.K. Nanda, One-step, integrated fabrication of Co_2P nanoparticles encapsulated N, P dual-doped CNTs for highly advanced total water splitting, Nano Energy 30 (2016) 303–311.
[24] Y. Zhang, Z.X. Hui, H.Y. Zhou, S.F. Zai, Z. Wen, J. Chen, Li, C.C. Yang, Q. Jiang, Ga doping enables superior alkaline hydrogen evolution reaction performances of CoP, Chem. Eng. J. 429 (2022), 132012.
[25] M. Zhuang, X. Ou, Y. Dou, L. Zhang, Q. Zhang, R. Wu, Y. Ding, M. Shao, Z. Luo, Polymer-embedded fabrication of Co_2P nanoparticles encapsulated in N,P-doped graphene for hydrogen generation, Nano Lett. 16 (2016) 4691–4698.
[26] V.H. Hoa, D.T. Tran, S. Prabhakaran, D.H. Kim, N. Hameed, H. Wang, N.H. Kim, J. H. Lee, Ruthenium single atoms implanted continuous MoS_2-Mo_2C heterostructure for high-performance and stable water splitting, Nano Energy 88 (2021), 106277.
[27] T. Gu, R. Sa, L. Zhang, D.-S. Li, R. Wang, Engineering interfacial coupling between Mo_2C nanosheets and Co@NC polyhedron for boosting electrocatalytic water splitting and zinc-air batteries, Appl. Catal. B Environ. 296 (2021), 120360.
[28] Y. Xu, J. Yang, T. Liao, R. Ge, Y. Liu, J. Zhang, Y. Li, M. Zhu, S. Li, W. Li, Bifunctional water splitting enhancement by manipulating Mo-H bonding energy of transition metal-Mo_2C heterostructure catalysts, Chem. Eng. J. 431 (2022), 134126.
[29] Q. Yuan, W. Chen, R. Hu, X. Chen, Z. Jiang, Metal-polydopamine derived N-doped carbon nanorod wrapping Ni and Mo_2C nanoparticles for efficient hydrogen evolution reaction, Mater. Lett. 307 (2022), 130989.
[30] S. Jin, Z. Shi, H. Jing, L. Wang, Q. Hu, D. Chen, N. Li, A. Zhou, Mo_2C-MXene/CdS heterostructures as visible-light photocatalysts with an ultrahigh hydrogen production rate, ACS Appl. Energy Mater. 4 (2021) 12754–12766.
[31] W. Yaseen, M. Xie, B.A. Yusuf, Y. Xu, N. Ullah, M. Rafiq, A. Ali, J. Xie, Synergistically coupling of Co/Mo_2C/$Co_6Mo_6C_2$@C electrocatalyst for overall water splitting: The role of carbon precursors in structural engineering and catalytic activity, Appl. Surf. Sci. 579 (2022), 152148.
[32] L. Wang, S. Zhao, Y. Liu, D. Liu, J.M. Razal, W. Lei, Interfacial engineering of 3D hollow Mo-based carbide/nitride nanostructures, ACS Appl. Mater. Interfaces 13 (2021) 50524–50530.
[33] X. Luo, Q. Zhou, S. Du, J. Li, L. Zhang, K. Lin, H. Li, B. Chen, T. Wu, D. Chen, M. Chang, Y. Liu, One-dimensional porous hybrid structure of Mo_2C-CoP encapsulated in N-doped carbon derived from MOF: an efficient electrocatalyst for hydrogen evolution reaction over the entire pH range, ACS Appl. Mater. Interfaces 10 (2018) 42335–42347.
[34] Y. Liu, K. Ai, L. Lu, Polydopamine and its derivative materials: synthesis and promising applications in energy, environmental, and biomedical fields, Chem. Rev. 114 (2014) 5057–5115.
[35] H. Lee, S.M. Dellatore, W.M. Miller, P.B. Messersmith, Mussel-inspired surface chemistry for multifunctional coatings, Science 318 (2007) 426–430.
[36] F.X. Ma, H.B. Wu, B.Y. Xia, C.Y. Xu, X.W. Lou, Hierarchical beta-Mo_2C nanotubes organized by ultrathin nanosheets as a highly efficient electrocatalyst for hydrogen production, Angew. Chem. Int. Ed. Engl. 54 (2015) 15395–15399.
[37] C. Wang, L. Sun, F. Zhang, X. Wang, Q. Sun, Y. Cheng, L. Wang, Formation of Mo-polydopamine hollow spheres and their conversions to MoO_2/C and Mo_2C/C for efficient electrochemical energy storage and catalyst, Small 13 (2017) 1701246.
[38] Y. Huang, Q. Gong, X. Song, K. Feng, K. Nie, F. Zhao, Y. Wang, M. Zeng, J. Zhong, Y. Li, Mo2C nanoparticles dispersed on hierarchical carbon microflowers for efficient electrocatalytic hydrogen evolution, ACS Nano 10 (2016) 11337–11343.
[39] H. Liu, J. Guan, S. Yang, Y. Yu, R. Shao, Z. Zhang, M. Dou, F. Wang, Q. Xu, Metal-organic-framework-derived Co_2P nanoparticle/multi-doped porous carbon as a trifunctional electrocatalyst, Adv. Mater. 32 (2020) 2003649.
[40] D. Sun, S. Lin, Y. Yu, S. Liu, F. Meng, G. Du, B. Xu, One-pot synthesis of N and P Co-doped carbon layer stabilized cobalt-doped MoP 3D porous structure for enhanced overall water splitting, J. Alloy. Compd. 895 (2022), 162595.
[41] P. Babar, A. Lokhande, H.H. Shin, B. Pawar, M.G. Gang, S. Pawar, J.H. Kim, Cobalt iron hydroxide as a precious metal-free bifunctional electrocatalyst for efficient overall water splitting, Small 14 (2018) 1702568.
[42] J. Zhang, Q. Zhang, X. Feng, Support and interface effects in water-splitting electrocatalysts, Adv. Mater. 31 (2019) 1808167.
[43] Y. Luo, Z. Zhang, M. Chhowalla, B. Liu, Recent advances in design of electrocatalysts for high-current-density water splitting, Adv. Mater. (2021) 2108133.
[44] F. Dionigi, J. Zhu, Z. Zeng, T. Merzdorf, H. Sarodnik, M. Gliech, L. Pan, W.X. Li, J. Greeley, P. Strasser, Intrinsic electrocatalytic activity for oxygen evolution of crystalline 3d-transition metal layered double hydroxides, Angew. Chem. Int. Ed. Engl. 60 (2021) 14446–14457.
[45] M. Tahir, L. Pan, F. Idrees, X. Zhang, L. Wang, J.-J. Zou, Z.L. Wang, Electrocatalytic oxygen evolution reaction for energy conversion and storage: A comprehensive review, Nano Energy 37 (2017) 136–157.

[46] Y. Wang, S. Li, D. Zhang, F. Tan, L. Li, G. Hu, Self-supported hierarchical P,Cu-codoped cobalt selenide nanoarrays for enhanced overall water splitting, J. Alloy. Compd. 889 (2021), 161696.
[47] X. Han, X. Wu, Y. Deng, J. Liu, J. Lu, C. Zhong, W. Hu, Ultrafine Pt nanoparticle-decorated pyrite-type CoS_2 nanosheet arrays coated on carbon cloth as a bifunctional electrode for overall water splitting, Adv. Energy Mater. 8 (2018) 1800935.
[48] H. Liu, G. Xia, R. Zhang, P. Jiang, J. Chen, Q. Chen, MOF-derived RuO_2/Co_3O_4 heterojunctions as highly efficient bifunctional electrocatalysts for HER and OER in alkaline solutions, RSC Adv. 7 (2017) 3686–3694.
[49] Y. Guo, P. Yuan, J. Zhang, H. Xia, F. Cheng, M. Zhou, J. Li, Y. Qiao, S. Mu, Q. Xu, Co_2P–CoN double active centers confined in N-doped carbon nanotube: heterostructural engineering for trifunctional catalysis toward HER, ORR, OER, and Zn–air batteries driven water splitting, Adv. Funct. Mater. 28 (2018) 1805641.
[50] J. Ryu, N. Jung, J.H. Jang, H.-J. Kim, S.J. Yoo, In situ transformation of hydrogen-evolving CoP nanoparticles: toward efficient oxygen evolution catalysts bearing dispersed morphologies with Co-oxo/hydroxo molecular units, ACS Catal. 5 (2015) 4066–4074.